S. Afr. J. Chem., 2021, **75**, 91–97
https://journals.co.za/content/journal/chem/

Degradation of *o*-Chloranil Using Nanocrystalline-Cellulose/TiO_2 Composites *via* a Solar Photocatalytic Route

Vashen Moodley, Suresh Maddila, Sreekantha B. Jonnalagadda and Werner E. van Zyl*

School of Chemistry and Physics, University of KwaZulu-Natal, Westville Campus, Durban, 4000, South Africa.

Received 25 May 2020 , revised 29 September 2020, accepted 29 September 2020

ABSTRACT

Water pollution by organic pollutants is a continuous and increasing problem of global concern. In this paper, we developed a nanocrystalline cellulose (NCC) and titania (TiO_2) based nanocomposite for the photocatalytic degradation of *o*-chloranil *via* aqueous wet impregnation. Different NCC loadings (10, 20, 40, and 80%) were used, and several analytical and microscopy techniques characterised the NCC/TiO_2 catalyst. The efficiency of TiO_2 as a photo-catalyst was enhanced through the chiral nematic nature and potential charge carrier capacity of NCC, which lowered the rate of electron recombination. The NCC/TiO_2 material was used in the solar-driven photo-degradation of *o*-chloranil (3,4,5,6-tetrachloro-1,2-benzoquinone), a by-product of a commonly used pesticide. The successful decomposition of *o*-chloranil led to the successful identification of three breakdown products, namely 2,3-dichloro-4,5-dioxohex-2-enedoic acid (DCA), 2,3-dioxosuccinic acid (DSA) and oxalic acid (OA). The 20% NCC/TiO_2 catalyst was found to be optimum and showed excellent degradation and mineralisation of *o*-chloranil within 2 hours (~90% degradation after 2 hours or 0.00920 mols of the total 0.0102 mols). The degradation products were analysed and identified using GC-MS. The photo-catalyst offers many benefits, including ease of preparation, a low cost-factor, and high stability with no loss of activity.

KEYWORDS

nanocrystalline cellulose; o-chloroanil; photocatalyst; photo-degradation; titania

1. Introduction

Environmental pollution is a significant yet poorly controlled hazard of the modern world.[1] Managing the progress in the agricultural, medicinal, and energy sectors are essential to keep up with the needs and demands of an ever-growing anthropological population.[2] Greener processes are required for the production of environmentally friendly products. Research endeavours have shifted to eradicating and reducing existing environmental pollutants and are moving toward a sustainable society where green chemistry processes and environmental remediation are necessary.[3]

There has been a remarkable increase in the awareness of the toxic effects of numerous polluting chemicals that were not considered hazardous only two decades ago.[4] One such pollutant has been identified as *o*-chloranil (3,4,5,6-tetrachloro-1,2-benzoquinone), which was observed as an oxidation by-product of pentachlorophenol (PCP). In the past, *o*-chloranil was used as a fungicide and algicide and was found to be genotoxic. Although banned, it is still used in a few countries and efforts to remediate the soil are underway.[5] Control of organic pollutants in water sources is an essential measure of environmental protection. In this regard, biodegradation pathways have garnered attention amongst the proposed and developed processes to eliminate organic contaminants.[4]

Photocatalysis signifies the catalysis of a photochemical reaction at a solid surface interface, usually in the form of a semiconductor.[6–16] This simplified definition, while correct and convenient, conceals that there must be at least two other reactions occurring concurrently. The first involves oxidation from photo-generated holes, while the second requires reduction from photo-generated electrons. During both processes, there must be an equal balance in a precise order for the preservation of the photocatalyst.[13, 15, 17, 18]

Heterogeneous photocatalysis has proven to be an efficient tool for degrading both aquatic and atmospheric organic contaminants. Such catalysts can be successfully applied to the photocatalytic oxidation for the partial or total mineralisation of pollutants into benign substances.[19] Photocatalytic degradation encompasses the use of certain semiconductors as catalysts for the production of highly reactive radicals under light/solar irradiation.[11, 20] As a semiconductor, TiO_2 is known to have a large band-gap, high surface area and offers excellent stability. It can be regarded as non-toxic and has a highly porous framework (with pores ranging from 2–50 nm in diameter).[21, 22] These characteristics make it a suitable material for photocatalysis.[22] The structure of TiO_2 has distinctive physical-chemical properties, which allows for the transfer of electrons within the material, and enables the simple recovery of the catalyst.[23] TiO_2 possesses a wide band-gap energy (3.2 eV) and requires electromagnetic radiation with equal or higher photon energy to excite electrons within the valence band (VB) to the conduction band (CB). This photon-induced excitation leaves holes within the VB. The recombination of electrons (e^-) and holes (h^+) initiates redox reactions, which allows a molecular species to be adsorbed onto the surface of the catalyst.[24, 25] Due to the wide band-gap energy and high electron-hole recombination rate, only ultraviolet irradiation ($\lambda < 387$ nm) possesses sufficient energy to overcome these shortcomings. This limits the application of TiO_2 under visible light conditions. Therefore TiO_2 is typically deposited on a support, which could enhance the separation of electron-hole pairs and in turn reduces electron-hole recombination rates, thereby increasing the photocatalytic efficiency of TiO_2 as a photo-catalyst.[26] The ideal support leads to a composite material that can act as a trap-site for the photo-generated electrons, preventing electron-hole recombination, thereby improving photocatalytic activity.[18] Recent reports have shown several support materials that promote the photocatalytic activity of TiO_2. These include TiO_2 doped carbon nanotubes,

*To whom correspondence should be addressed
Email: vanzylw@ukzn.ac.za

ISSN 1996-840X Online / South African Chemical Institute / http://saci.co.za/journal

https://doi.org/10.17159/0379-4350/2021/v75a10

TiO_2/zeolite composites, TiO_2/activated carbon composites, and TiO_2/graphene oxide composites.[27–30]

Photocatalysed oxidative mineralisation is a promising chemical process that leads to the degradation of organic pollutants.[31] The photocatalytic oxidation-based systems have been developed to take advantage of the hydroxyl radical (•OH) production.[32] In an aqueous TiO_2 suspension, water molecules are oxidised to •OH by photo-generated positive holes and then react with organic compounds to form oxidised species and decomposed products.[33–36] During this process, carbonyl compounds and carboxylic acids are created *via* the degradation step. However, the oxidative reaction is not rapid; thus, the radical formation step is executed. The reaction of the •OH radical with pollutants is an immediate process, and therefore reaction conditions need to be considered. The catalyst surface basicity and acidity plays a vital role in terms of, for example, the point of zero charge during the process.[37, 38]

Cellulose-based TiO_2 composites have shown enhancement[39] of the light absorption properties over bare TiO_2. Further studies have illustrated that nano-sized cellulose particles have proven to be an ideal support for TiO_2 with an improvement of its photocatalytic properties.[40–43] Nanocrystalline cellulose (NCC) is a chiral nematic material with potential photonic use, leading to iridescent coloured films. This biopolymer was chosen as a second phase in the nanocomposite.[44, 45] Chiral nematic NCC could act as a potential charge carrier, and in turn, increase the efficiency of TiO_2 as a photo-catalyst by lowering the rate of electron recombination as well as aiding in the adsorption of organic substrates to the surface of the catalyst. An NCC/TiO_2 nanocomposite, therefore, appears to be a promising material for the photocatalytic decomposition of organic pollutants.

This study demonstrates the facile fabrication of a hybrid NCC/TiO_2 nanocomposite by the wet impregnation of TiO_2 (anatase) nanoparticles on NCC. The NCC was isolated from bleached pulp *via* acid hydrolysis (64 wt% H_2SO_4). The prepared nanocomposites were characterised using different techniques. These techniques include powder X-ray diffraction (PXRD), Fourier-transform infrared (FT-IR) spectroscopy, scanning electron microscopy (SEM), transmission electron microscopy (TEM), specific surface area and porosity measurements and optical spectroscopic analysis. After characterisation, the composite material was used in the photocatalytic degradation of *o*-chloranil. The degradation product was then analysed with mass spectrometry, and a reaction mechanism was proposed.

2. Materials and Methods

2.1. Materials

Bleached hardwood pulp was provided by the CSIR, Durban, South Africa. Ethanol, sodium hydroxide pellets, sulfuric acid, and titania (anatase) were purchased from Sigma-Aldrich. *o*-Chloranil was purchased from BDH Chemicals (Merck). All chemicals were used as received. Double distilled water was used for all reactions and dialysis.

2.2. Photocatalytic study

The photo-degradation of *o*-chloranil with a fixed absorbance of 0.3281 (a.u.) at a λ_{max} of 298 nm was undertaken. The light source used was natural sunlight to mimic real-world conditions (26°C on a clear day). Light intensity was determined using a Kipp and Zonen CHP1 pyrheliometer attached to the Solys2 automatic sun tracker.[46] The average measured intensity of the sun was 602.511 Wm^{-2}.

A 2 L aqueous solution of *o*-chloranil (10 ppm) was prepared and sonicated for 10 mins to allow the total dissolution of *o*-chloranil. The *o*-chloranil solution (250 mL) was then added to an 800 mL beaker containing 100 mg of catalyst (control, bare TiO_2, NCC/TiO_2 (10%, 20%, 40% and 80% w/w%) and pure NCC). Initial absorbance measurements were taken 60 min before data collection started in a dark room, with the set-up moved to the reaction site in the dark. The reaction was stirred for 120 minutes, with absorbance measurements taken every 20 minutes.

2.3. Catalyst preparation

Cellulose was isolated from the bleached pulp (BP) following blending. The NCCs were isolated using 20 $mL.g^{-1}$ 64 wt% sulfuric acid at 45°C in an oil bath for 45 minutes to remove the amorphous regions. After completing the hydrolysis, the suspensions were repeatedly diluted and centrifuged at 6000 rpm for 10 minutes to reduce the sulfuric acid concentration. The suspensions were later sonicated using a UP400S Ultrasonic processor (Hielscher, Germany) at 50% amplitude and 0.5 cycles for 15 minutes to ensure complete dispersion of NCCs before dialysis to near-neutral pH. The obtained NCCs were denoted as NCC-BP.[47]

The photo-catalysts were prepared by the wet impregnation method. TiO_2 (0.9, 0.8, 0.6, and 0.2 g) was suspended in 50 mL of deionised water with vigorous stirring for 30 minutes. NCC (prepared, 0.1, 0.2, 0.4 and 0.8 g) was then added with additional stirring for 60 minutes. The pH was subsequently adjusted to 8.5 using a 0.1 M NaOH solution. The suspension was vigorously stirred for a further 2 hours. The suspensions were heated at 60-70°C for 2 hours. The samples were then sonicated, filtered, and washed with deionised water. The suspensions were dried at 90-100°C overnight to obtain the 10%, 20%, 40, and 80% w/w% of NCC/TiO_2 catalysts.

2.4. Characterisation techniques

2.4.1. Mass spectral analysis

The GC-MS analysis was done in EI mode using a Perkin Elmer Clarus 400 Gas Chromatograph equipped with an EI mode mass spectra photometer. The spectra were recorded in the interval 35–500 amu. Specification of the column used was as follows: J & W DB5MS, 30 m length, 250 μm diameter and 0.25 μm film thickness. Helium was used as the carrier gas, and the temperature ramp program used during GC analysis was as follows: 50°C (2 minutes), then 20°C min^{-1} to 300°C (10 minutes). Compounds were matched to the NIST Mass Spectrometry Data Center Library.

The mass spectra were recorded on an Agilent 1100 LC/MSD instrument, with method API-ES, at 70 eV.

2.4.2. Optical spectroscopic analysis

The materials were analysed using a Perkin Elmer LS 55 fluorescence spectrophotometer, for which the samples were excited with high photon energy at 310 nm. UV-visible diffuse reflectance spectra were recorded with an Ocean Optics high-resolution spectrometer (HR2000+) equipped with an integrating sphere accessory, using $BaSO_4$ as the reference material.

2.4.3. Fourier-transform infrared spectroscopy

The NCC/TiO_2 was analysed by FTIR in the range 380-4000 cm^{-1} at a resolution of 4 cm^{-1} using a Spectrum 100 infrared spectrometer equipped with a universal attenuated total reflection (UATR) accessory (Perkin Elmer, USA).

2.4.4. Morphological structure analysis

The morphological characterisation, dimensions and elemental composition of the NCC/TiO_2 catalyst were established with electron microscopic studies using a JEOL 1010 (Japan) transmission electron microscope (TEM) and a ZEISS Ultra Plus (Germany) field emission gun scanning electron microscope (FEG-SEM) equipped with energy dispersive X-ray (EDX) detector. The emission current using a tungsten (W) filament was 100 μA, and the accelerator voltage was 12 kV.

TEM images of all samples were acquired using the NCC/TiO_2 catalysts deposited on the TEM-grid. The TEM-grids were also negatively stained with uranyl acetate to aid visualisation of NCC with the NCC/TiO_2 catalysts matrix. Similarly, samples for SEM images were coated with gold with the aid of a sputter coater to minimise charging.

2.4.5. X-ray diffraction analysis

Powder X-ray diffraction (XRD) analysis of the NCC/TiO_2 catalyst was conducted using an X-ray diffractometer (Bruker AXS D8 Advance, Germany), equipped with Cu-Kα radiation source (wavelength = 0.154 nm) operating at 40 kV and 40 mA. The XRD pattern of the catalyst was recorded over the angular range 2θ = 10 – 90° at room temperature.

Crystallite size (D_{hkl}) of the isolated NCC/TiO_2 was calculated using Scherrer's formula, as shown in Equation (1)

$$D_{hkl}\,(\text{nm}) = 0.94\lambda/\beta \cos\theta \quad (1)$$

where λ is the X-ray wavelength (0.154 nm), β is the angular width at a half-maximum intensity, and θ is the Bragg angle.

2.4.6. Specific surface area and porosity measurements

The nitrogen adsorption-desorption isotherms of the degassed samples were recorded at 100°C under vacuum for 24 h using a Micromeritics VacPrep 061 (USA) sample degas system and were measured at a bath temperature of -195.8 °C (77.2 K) by a surface area and porosity analyser, Micromeritics Tristar II 3020 2.00, USA. Specific surface areas were calculated from the linear region of the isotherms using the Brunauer–Emmett–Teller (BET) equation in a relative P/Po pressure range of 0.058–0.8. Pore size distributions were derived from the adsorption branch of the isotherms by the Barrett–Joyner–Halenda (BJH) method. The total pore volumes were estimated from the amount adsorbed at a relative pressure of P/P_o = 0.996.

3. Results and Discussion

3.1. FT-IR analysis

The FT-IR spectrum of the prepared NCC/TiO_2 photo-catalysts and NCC and TiO_2 are shown in Figure 1. The sequence of bands seen in these spectra corresponds to the various lattice vibrational modes of NCC and TiO_2. The bands at 1030 and 1415 cm^{-1} display -CH3 and O-H vibrational stretching modes, which were attributed to the presence of NCC.[48] The two bands at 599 cm^{-1} and 776 cm^{-1} correspond to TiO_2.[49, 50] The broad bands in the range of 3000–3441 cm^{-1} were attributed to surface hydroxyl group peaks. The peak at 1628 cm^{-1} was attributed to water absorbed on NCC.[51]

3.2. BET surface and elemental analysis

The N2 sorption study was carried out over bare TiO_2 and the NCC/TiO_2 catalysts (Figure S1). N2 sorption resulted in typical type IV isotherm, with a narrow H_2 hysteresis loop lying in the P/P0 range of 0.85–0.95, demonstrating a marginally porous character.[52]

The BET surface areas of bare TiO_2, 10%, 20 %, 40 %, and 80% NCC/TiO_2 catalysts were 8.58, 10.62, 10.08, 10.57, 1.96 $m^2.g^{-1}$, respectively. These results may be attributed to the macropores caused by particle-particle porosity (inter-particle porosity). The prepared catalysts also exhibit a step increase at this relative pressure range due to the filling of interparticle macropores of the catalyst with nitrogen.[53] The isotherms and pore size distributions remained essentially unchanged over the range of NCC concentrations, which implies that the NCC-containing species did not significantly disturb the pore structure of TiO_2.[54] There was a moderate change in the surface area from the TiO_2 to the NCC/TiO_2 catalyst. A drastic decrease in surface area and pore volume was observed as the NCC dopant became the major component (Table 1) attributed to the virtually non-porous NCC.

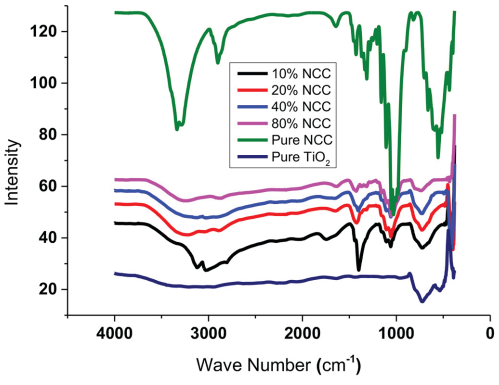

Figure 1 ATR-FTIR spectra of prepared NCC/TiO_2 photo-catalysts.

3.3. SEM and TEM analysis

The transmission electron microscopy (TEM) micrographs of bare TiO_2, 10%, 20 %, 40 %, and 80% NCC/TiO_2 catalysts (Figure 2) showed disc-shaped particles with sizes ranging between 100 – 130 nm in diameter (Figure S2). The size of TiO_2 particles deposited on the NCC catalysts showed no significant changes when compared to the neat TiO_2 particles. However, strand/bone-like NCC particles were evident upon the samples' staining (Figure 2b, 2d, 2f, and 2h). The sizes of NCC rods ranged between 100 – 250 nm in length. With the introduction of NCC into the TiO_2 matrix, the spherical particles appeared to have aggregated, forming clusters on the NCC particles. This aggregation is attributed to NCC/TiO_2 and NCC/NCC interactions during the catalyst's drying.[55–57]

The particles were large, with an irregular elliptical shape as observed by a field emission SEM micrograph (Figure 3). The micrographs showed that the TiO_2 particles were in an aggregated state and adhered to the NCC rods. A homogeneous distribution of smaller TiO_2 particles was seen on the surface of larger TiO_2 particles (Figure 3g-h). The EDS mapping quantified this phenomenon (Figure 4), and the morphology of the catalyst additionally points to a semi-crystalline and homogenous sample.

3.4. XRD analysis

The prepared catalysts showed the presence of the TiO_2 anatase phase. The diffraction peaks located at 2θ = 25.2°, 37.9°, 48.0°, and 62.0° were indexed to (101), (004), (200) and (204) planes of anatase phase TiO_2 (Figure 5).[19, 58] The increase in the NCC loading was shown by a slight peak shift in the XRD diffractogram at 2θ = 16° and 22°. By increasing in NCC loading, there was no evidence of an increase in the NCC peaks. This occurrence was attributed to the high crystallinity of TiO_2, which masks the NCC peaks.

The average crystallite size of the catalysts was determined by the Scherrer equation using the full-width at half-maximum (FWHM) of the peak corresponding to the (101) reflection. It was found that the sizes for 10%, 20%, 40%, and 80% loadings were *ca.* 44.4, 44.0, 27.6, and 16.6 nm, respectively. Ultra-sonication leads to a decrease in crystallite size. Because NCC is a softer

Table 1 Surface area and pore volumes of synthesised catalysts.

Catalyst	Surface area $m^2.g^{-1}$	Pore Volume $cm^3.g^{-1}$
Pure Titania	8.58	0.104
10% NCC/Titania	10.62	0.049
20% NCC/Titania	10.08	0.060
40% NCC/Titania	10.57	0.069
80% NCC/Titania	1.96	0.029

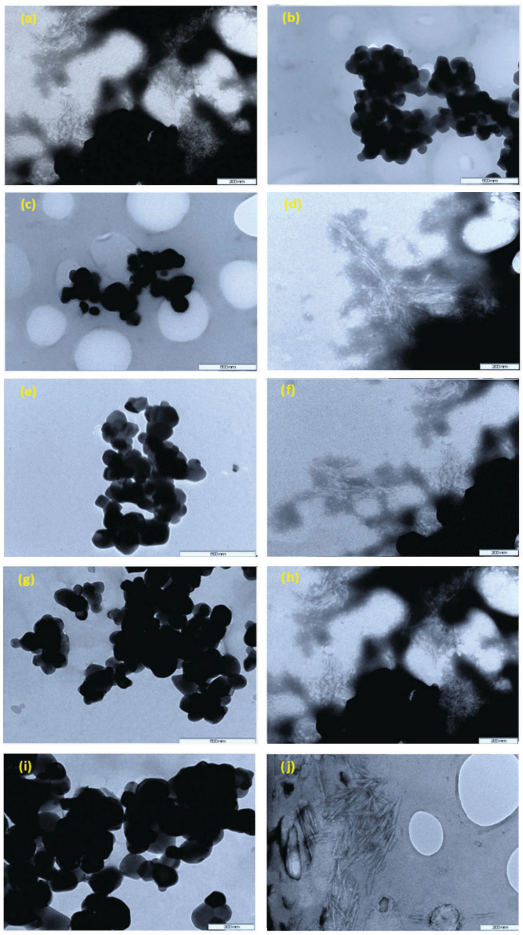

Figure 2 TEM micrographs of unstained and stained 10% (2a–2b), 20% (2c–2d), 40% (2e–2f) and 80% (2g–2h) NCC/TiO2 catalysts. Bare TiO2 (2i) and NCC (2j) are shown.

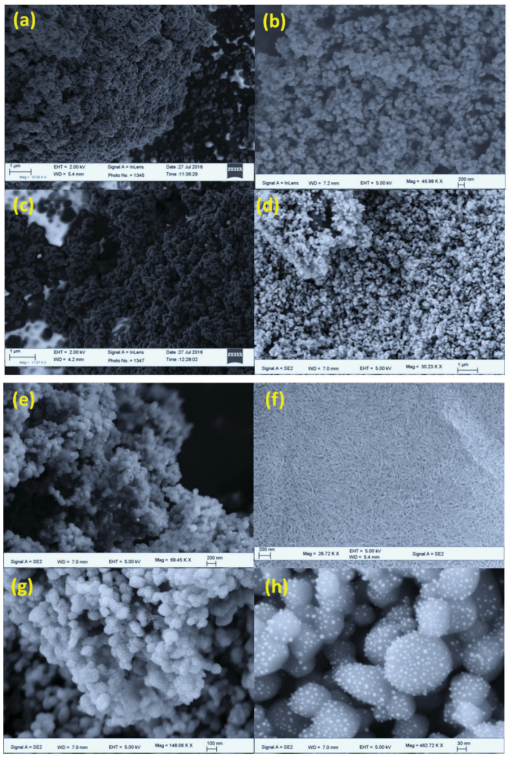

Figure 3 SEM micrographs of 10%, 20%, 40% and 80% (a-d) NCC/TiO_2 catalysts. Bare TiO_2 (e) and NCC (f). 100K and 450K magnification, respectively (g–h).

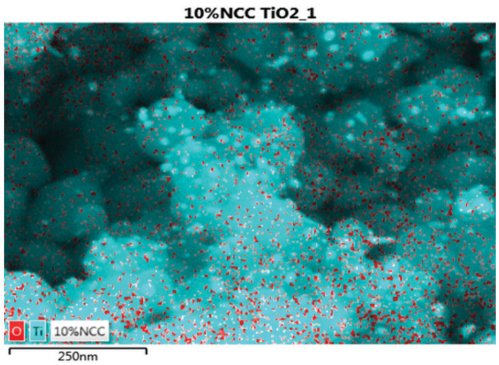

Figure 4 SEM-EDX mapping of 10% NCC/TiO_2.

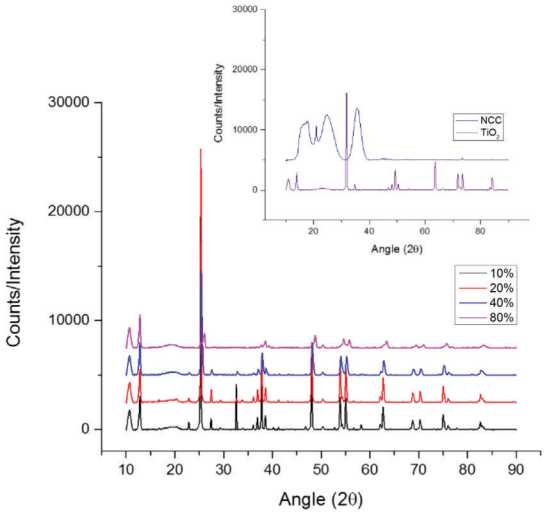

Figure 5 The PXRD pattern of (inset) pure NCC bare TiO2 (anatase), 10%, 20%, 40% and 80% NCC–TiO_2.

material than TiO_2, the higher the NCC loading, the smaller the catalyst particles become. The increase in NCC loading led to an increase in the dispersion of the TiO_2. This increase in distribution allowed for a more significant fracture in the catalyst.[59]

3.5. UV-diffuse reflectance spectra

The thick absorption band at ca. 372 nm (Figure S3) conforms to band-gap energy of 3.21 eV calculated from the formula $E_g = 1239.8/\lambda$.[13, 60] Upon doping with NCC, a red-shift was observed, which could aid the catalyst's photocatalytic activity under visible light.

3.6. Photoluminescence spectra

The PL spectra (Figure 6) of NCC/TiO_2 samples range between 350–500 nm with an excitation wavelength of 360 nm. The PL spectra are related to the recombination of photoinduced electrons and holes and free and self-trapped excitons, which possibly generate from surface defects in the TiO_2 crystals, such as lattice distortions and surface oxygen deficiencies.[33–36] The spectra illustrate that an increase in NCC loading led to a decrease in intensity. This decrease indicated the reduction of the recombination centres for the electrons and holes in the samples and suggested that the NCC/TiO_2 catalysts led to low rates of electron-holes recombination under light irradiation and may show better photocatalytic activity than bare TiO_2.[36]

3.7. Catalyst loading concentration

The photo-catalyst loading was increased from 50 mg.L^{-1} to 200 mg.L^{-1} (Figure 7). The 100 mg.L^{-1} catalyst load was the

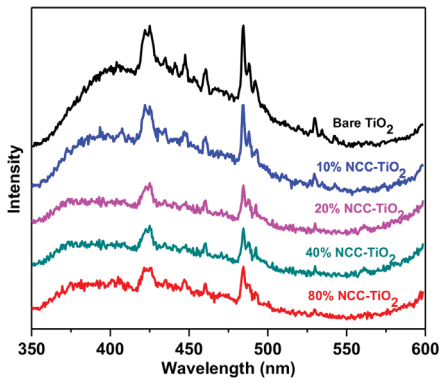

Figure 6 Photoluminescence spectra of bare TiO_2 and the synthesised (% w/w) NCC/TiO_2 catalysts

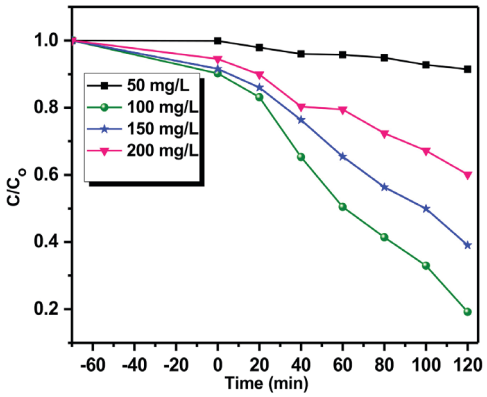

Figure 7 Influence of the amount of catalyst (NCC/TiO_2 with 20% NCC doping) loading on the o-chloranil photo-degradation.

most efficient for *o*-chloranil photo-degradation. When the catalyst concentration increased, the reaction rate decreased. We propose this is due to the lack of accessibility of sufficient catalytic active sites on the catalyst material surface and the penetration of light into the suspension.

3.8. Degradation of o-chloranil

The degradation of *o*-chloranil as a function of time using the synthesised catalysts, bare NCC, and pure TiO_2 under visible light, and after equilibrating in the dark for 1 hour, is shown in Figure 8. The catalyst of NCC/TiO_2 with 20% NCC doping displayed the highest photocatalytic activity due to the ability of nanocellulose assisting in the capture of electrons to achieve a higher photocatalytic activity with a suitable doping concentration.[13, 15]

With an increase in cellulose dopant concentration, recombination of photo-generated electron-hole pairs may decrease photocatalytic activity. Therefore, a higher loading of NCC >20 wt% was not required.

3.9. Identification of products

All the photo-catalysed investigations were accompanied by exposing the reaction mixture to visible light. The organic portion of the reaction mixture was extracted and analysed after every reaction with 20-minute intervals. Three products were identified by gas chromatography (GC) after 120 min (Figure S4a).

After GC-MS injection, peaks were observed with retention times at 15.807, 13.558, and 8.507 minutes were confirmed and refer to 2,3-dichloro-4,5-dioxohex-2-enedoic acid (DCA),

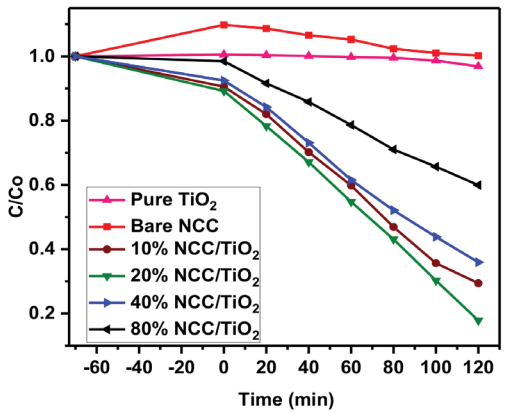

Figure 8 The photo-degradation *o*-chloranil as a function of time

2,3-dioxosuccinic acid (DSA) and oxalic acid (OA), respectively. Furthermore, the formation of these products was confirmed by LC-MS with their respective (M^+) m/z values (Figure S4b,c,d).

3.10. Reaction mechanism

Based on the previous results, a possible reaction mechanism (Scheme 1) for the photocatalytic degradation of *o*-chloranil is proposed.

In an aromatic substituted compound, chloro functional groups are electron-withdrawing,[61, 62] and this reduction in electron density on the carbon atom make it susceptible to hydroxyl radical attack. This attack leads to the elimination of chlorides and a subsequent ring-opening—a consequent attack by the •OH radical causes the formation of an aliphatic acid. The short-lived intermediate, DCA, favours the electrophilic substitution of •OH at the supplementary chloro position and forms a dechlorinated species through photo-oxidation. The further oxidation of the intermediate by •OH leads to oxygenated aliphatic compounds and the formation of degraded aliphatic carboxylic acids. Two aliphatic acids (DSA and OA) were identified in this study. Further oxidation of these acid products leads to complete mineralisation to the final products of CO_2 and H_2O.

4. Conclusions

This study shows that the NCC/TiO_2 catalyst could efficiently catalyse the photo-degradation and mineralisation of the

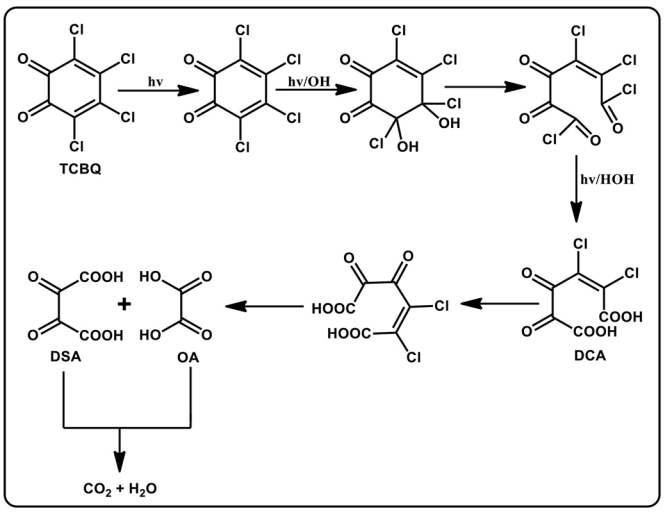

Scheme 1 The proposed mechanism for the photo-degradation of *o*-chloranil

pollutant *o*-chloranil in the presence of sunlight. Using a wet-impregnation method, materials with different loadings of NCC on TiO_2 catalysts were successfully produced. The NCC/TiO_2 composite allowed for the capture of photo-holes, retarding the recombination of photo-generated electron-hole pairs relative to pure TiO_2, which helped in the adsorption of the pollutant onto the surface of the catalyst. Overall the 20 %w/w NCC/TiO_2 proved to be the most efficient catalyst for solar photocatalysed degradation of *o*-chloranil. The results show that the degradation rate can be influenced by various parameters, such as NCC concentration and photo-catalyst loading. The intermediate product (DCA) formed during the process could be responsible for the slow mineralisation of the model pollutant and contributes helpful information to the degradation pathway. The investigation strongly suggests that DCA, DSA, and OA are the primary intermediates formed during the model contaminant's photo-degradation. NCC/TiO_2 provides a cheap and facile means to produce a photo-catalyst that can be employed for the degradation of harmful pollutants. Although this was a simulated solution study, most soil contaminants are washed away to water sources. A real-world experimental approach to identify contaminants within agricultural water sources and applying the catalysts in a batch process would provide useful information.

Acknowledgements

The authors thank the UKZN Nanotechnology Platform initiative for research facilities. For financial assistance, we thank the National Research Foundation, South Africa (Grant #95799), the Eskom TESP Programme (Grant #P677), and the Forestry and Forest Products Research Center at the CSIR, Durban, for providing dissolved hardwood pulp.

Supplementary Material

Supplementary information for this article is provided in the online supplement.

ORCID iD

Vashen Moodley: https://orcid.org/0000-0002-8851-8087
Suresh Maddila: https://orcid.org/0000-0001-5183-2104
S.B. Jonnalagadda: https://orcid.org/0000-0001-6501-8875
Werner E. van Zyl: https://orcid.org/0000-0002-2012-8584

References

1 W.A. Suk, K. Murray, M.D. Avakian, Environmental hazards to children's health in the modern world, *Mutat. Res./Rev. Mutat. Res.*, 2003, **544**, 235–242.

2 M.E. Colby, Environmental management in development: The evolution of paradigms, *Ecol Econ.*, 1991, **3**, 193–213.

3 J. Fiksel, Designing resilient, sustainable systems, *Environ. Sci. Technol.*, 2003. **37**, 5330–5339.

4 I. Dincer, Energy and environmental impacts: Present and future perspectives, *Energy Sources*, 1998, **20**, 427–453.

5 D. H. Sarr, C. Kazunga, M. J. Charles, J. G. Pavlovich, & M. D. Aitken, Decomposition of tetrachloro-1, 4-benzoquinone (P-chloranil) in aqueous solution. *Environ. Sci. Technol.*, 1995, **29**, 2735–2740.

6 E. Pelizzetti, and N. Serpone, eds. *Homogeneous and heterogeneous photocatalysis*, Vol. **174**. Springer Science & Business Media, 2012.

7 N. Serpone, E. Pelizzetti, *Photocatalysis: Fundamentals and applications*, Wiley-Interscience, 1989.

8 P.V. Kamat, Photochemistry on nonreactive and reactive (semiconductor) surfaces, *Chem. Rev.*, 1993, **93**, 267–300.

9 D.F. Ollis, H. Al-Ekabi, *Photocatalytic purification and treatment of water and air, Proceedings of the 1st International Conference on TiO_2 Photocatalytic Purification and Treatment of Water and Air, London, Ontario, Canada*, 8–13 November 1992. Elsevier Science Ltd, 1993.

10 A. Heller, Chemistry and applications of photocatalytic oxidation of thin organic films, *Acc. Chem. Res.*, 1995 **28**, 503–508.

11 M.R. Hoffmann, S.T. Martin, W. Choi, D.W. Bahnemann, Environmental applications of semiconductor photocatalysis, *Chem. Rev.*, 1995 **95**, 69–96.

12 A. Mills, S. Le Hunte, An overview of semiconductor photocatalysis, *J. Photochem Photobiol. A. Chem.*, 1997, **108**, 1–35.

13 A. Fujishima, K. Hashimoto, T. Watanabe, *TiO_2 photocatalysis: fundamentals and applications,* BKC Incorporated, 1999.

14 D.A. Tryk, A. Fujishima, K. Honda, Recent topics in photoelectrochemistry: Achievements and future prospects, *Electrochim. Acta.*, 2000 **45**, 2363–2376.

15 A. Fujishima, X. Zhang, Titanium dioxide photocatalysis: Present situation and future approaches, *C. R. Chim.*, 2006, **9**, 750–760.

16 A. Fujishima, X. Zhang, D.A. Tryk, Heterogeneous photocatalysis: From water photolysis to applications in environmental cleanup, *Int. J. Hydrogen Energy*, 2007, **32**, 2664–2672.

17 A. Fujishima, T.N. Rao, D.A. Tryk, Titanium dioxide photocatalysis, *J. Photochem. Photobiol.*, 2000 **1**, 1–21.

18 A. Fujishima, X. Zhang, D.A. Tryk, TiO_2 Photocatalysis and related surface phenomena, *Surf. Sci. Rep.*, 2008, **63**, 515–582.

19 E.C. Chetty, V.B. Dasireddy, S. Maddila, S.B. Jonnalagadda, Efficient conversion of 1,2-dichlorobenzene to mucochloric ccid with ozonation catalysed by V_2O_5 loaded metal oxides, *Appl. Catal. B.*, 2012 **117**, 18–28.

20 Y.-G. Zhang, L.-L. Ma, J.-L. Li, Y. Yu, *In situ* fenton reagent generated from TiO_2/Cu_2O composite film: A new way to utilise TiO_2 under visible light irradiation, *Environ. Sci. Technol.*, 2007, **41**, 6264–6269.

21 O. Lorret, D. Francová, G. Waldner, N. Stelzer, W-doped titania nanoparticles for UV and visible-light photocatalytic reactions, *Appl. Catal. B.*, 2009, **91**, 39–46.

22 P.A. Pekakis, N.P. Xekoukoulotakis, D. Mantzavinos, Treatment of textile dyehouse wastewater by TiO_2 photocatalysis, *Water Res.*, 2006, **40**, 1276–1286.

23 A. Ibhadon, P. Fitzpatrick, Heterogeneous photocatalysis: Recent advances and applications, *Catalysts*, 2013, **3**, 189.

24 M.A. Fox, M.T. Dulay, Heterogeneous photocatalysis, *Chem. Rev.*, 1993, **93**, 341–357

25 Y. Tamaki, A. Furube, M. Murai, K. Hara, R. Katoh, M. Tachiya, Direct observation of reactive trapped holes in TiO_2 undergoing photocatalytic oxidation of adsorbed alcohols: Evaluation of the reaction rates and yields, *J. Am. Chem. Soc.*, 2006, **128**, 416–417.

26 N. Venkatachalam, M. Palanichamy, V. Murugesan, Sol-gel preparation and characterisation of alkaline earth metal doped nano TiO_2: Efficient photocatalytic degradation of 4-chlorophenol, *J. Mol. Catal. A: Chem.*, 2007, **273**, 177–185.

27 Y.-J. Xu, Y. Zhuang, X. Fu, New insight for enhanced photocatalytic activity of tio_2 by doping carbon nanotubes: A case study on degradation of benzene and methyl orange, *J. Phys. Chem. C*, 2010, **114**, 2669–2676.

28 G. Zhang, A. Song, Y. Duan, S. Zheng, Enhanced photocatalytic activity of tio_2/zeolite composite for abatement of pollutants, *Micropor. Mesopor. Mater.*, 2018, **255**, 61–68.

29 B. Xing, C. Shi, C. Zhang, G. Yi, L. Chen, H. Guo, G. Huang, J. Cao, Preparation of TiO_2/activated carbon composites for photocatalytic degradation of RhB under UV light irradiation, *J. Nanomater.*, 2016, **10**.

30 P. Muthirulan, C. N. Devi, M. M. Sundaram, Fabrication And Characterization Of Efficient Hybrid Photocatalysts Based On Titania And Graphene For Acid Orange Seven Dye Degradation Under UV Irradiation, *Adv. Mater. Lett.*, 2014, **5**, 163–171.

31 F. Javier Benitez, J.L. Acero, F.J. Real, Degradation of carbofuran by using ozone, UV radiation and advanced oxidation processes, *J. Hazard. Mater.*, 2002, **89**, 51–65.

32 M.J. Farré, M.I. Franch, S. Malato, J.A. Ayllón, J. Peral, X. Doménech, Degradation of some biorecalcitrant pesticides by homogeneous and heterogeneous photocatalytic ozonation, *Chemosphere*, 2005, **58**, 1127–1133.

33 C.D. Jaeger, A.J. Bard, Spin trapping and electron spin resonance

detection of radical intermediates in the photodecomposition of water at titanium dioxide particulate systems, *J. Phys. Chem.*, 1979, **83**, 3146–3152.

34 N. Hiroyuki, O. Kazuo, O.-N Hiroaki, K. Hitoshi, Efficient hydroxyl radical production and their reactivity with ethanol in the presence of photoexcited semiconductors, *Bull. Chem. Soc. Jpn.*, 1994, **67**, 2031–2037.

35 G. Riegel, J.R. Bolton, Photocatalytic efficiency variability in TiO_2 particles, *J. Phys. Chem.*, 1995, **99**, 4215–4224.

36 Y. Nosaka, S. Komori, K. Yawata, T. Hirakawa, A.Y. Nosaka, Photocatalytic $^{-}$OH radical formation in TiO_2 aqueous suspension studied by several detection methods, *Phys. Chem. Chem. Phys.*, 2003, **5**, 4731–4735.

37 J.Y. Hu, Z.S. Wang, W.J. Ng, S.L. Ong, The effect of water treatment processes on the biological stability of potable water, *Water Res.*, 1999, **33**, 2587–2592.

38 E.C. Chetty, S. Maddila, C. Southway, S.B, Jonnalagadda, Ozone initiated ni/metal oxide catalyzed conversion of 1,2-dichlorobenzene to mucochloric acid in aqueous solutions, *Ind. Eng. Chem. Res.*, 2012, **51**, 2864–2873.

39 A. W. Morawski, E. Kusiak-Nejman, J. Przepiórski, R. Kordala, J. Pernak, Cellulose-TiO_2 nanocomposite with enhanced UV–Vis light absorption, *Cellulose*, 2013, **20**, 1293–1300.

40 Y. Luo, J. Xu, J. Huang, Hierarchical nanofibrous anatase-titania–cellulose composite and it's photocatalytic property, *CrystEngComm.*, 2014, **16**, 464–471.

41 Y. Luo, J. Huang, hierarchical-structured anatase-titania/cellulose composite sheet with high photocatalytic performance and antibacterial activity, *Chem. Eur. J.*, 2015, **21**, 2568–2575.

42 C. Schütz, J. Sort, Z. Bacsik, V. Oliynyk, E. Pellicer, A. Fall, L. Wågberg, L. Berglund, L. Bergström, G. Salazar-Alvarez, Hard and transparent films formed by nanocellulose TiO_2 nanoparticle hybrids, *PLoS One*, 2012, **7**, e45828.

43 J. Zeng, S. Liu, J. Cai, L. Zhang, TiO_2 immobilized in cellulose matrix for photocatalytic degradation of phenol under weak UV light irradiation, *J. Phys. Chem. C*, 2010, **114**, 7806–7811.

44 J.A. Kelly, M. Giese, K.E. Shopsowitz, W.Y. Hamad, M.J. MacLachlan, The development of chiral nematic mesoporous materials, *Acc. Chem. Res.*, 2014, **47**, 1088–1096.

45 Y. Zhou, C. Fuentes-Hernandez, T.M. Khan, J.-C. Liu, J. Hsu, J.W. Shim, A. Dindar, J.P. Youngblood, R.J. Moon, B. Kippelen, Recyclable organic solar cells on cellulose nanocrystal substrates, *Sci. Rep.*, 2013, **3**, 1536.

46 P. Govender, M. J. Brooks, A. P. Matthews, Cluster Analysis for classification and forecasting of solar irradiance in Durban, South Africa, *J. energy South. Afr.*, 2018, **29**, 63–76.

47 V. Moodley, S. Maddila, S. B. Jonnalagadda, W. E. van Zyl, Synthesis of triazolidine-3-one derivatives through the nanocellulose/hydroxyapatite-catalyzed reaction of aldehydes and semicarbazide, *New J. Chem.*, 2017, **41**, 6455–6463.

48 A. Kumar, Y.S. Negi, V. Choudhary, N.K. Bhardwaj, Characterisation of cellulose nanocrystals produced by acid-hydrolysis from sugarcane bagasse as agro-waste, *J. Mater. Phys. Chem.*, 2014, **2**, 1–8.

49 K. Nakamoto, *Handbook of vibrational spectroscopy*, John Wiley & Sons, Ltd., 2006.

50 R.A. Nyquist, R.O. Kagel, Handbook of Infrared and raman spectra of inorganic compounds and organic salts: Infrared spectra of inorganic compounds, Academic Press, **4**, 2012.

51 Y. Tang, S. Yang, N. Zhang, J. Zhang, Preparation and characterization of nanocrystalline cellulose via low-intensity ultrasonic-assisted sulfuric acid hydrolysis, *Cellulose*, 2014, **21**, 335–346.

52 Y. Kamiya, E. Nishikawa, A. Satsuma, M. Yoshimune, T. Okuhara, Highly porous vanadium phosphorus oxides derived from vanadyl n-butylphosphate, *Micropor. Mesopor. Mater.*, 2002, **54**, 277–283.

53 K. Bhattacharyya, S. Varma, A.K. Tripathi, S.R. Bharadwaj, A.K. Tyagi, Effect of vanadia doping and its oxidation state on the photocatalytic activity of TiO_2 for gas-phase oxidation of ethene, *J. Phys. Chem. C*, 2008, **112**, 19102–19112.

54 Y. Yang, S. Lim, C. Wang, D. Harding, G. Haller, Multivariate correlation and prediction of the synthesis of vanadium substituted mesoporous molecular sieves, *Micropor. Mesopor. Mater.*, 2004, **67**, 245–257.

55 M.A. Mohamed, W.N.W. Salleh, J. Jaafar, S.E.A.M. Asri, A.F. Ismail, Physicochemical properties of "green" nanocrystalline cellulose isolated from recycled newspaper, *RSC Adv.*, 2015, **5**, 29842–29849.

56 H.A. Silvério, W.P. Flauzino Neto, N.O. Dantas, D. Pasquini, Extraction and characterisation of cellulose nanocrystals from corncob for application as reinforcing agent in nanocomposites, *Ind. Crops Prod.*, 2013, **44**, 427–436.

57 P. Kampeerapappun, Extraction and characterisation of cellulose nanocrystals produced by acid hydrolysis from corn husk, *J. Miner. Metal Mater.*, 2015, **25**, 19–26.

58 Y. Luo, X. Liu, J. Huang, Heterogeneous nanotubular anatase/rutile titania composite derived from natural cellulose substance and its photocatalytic property, *CrystEngComm.*, 2013, **15**, 5586–5590.

59 J.C. Colmenares, M.A. Aramendía, A. Marinas, J.M. Marinas, F.J. Urbano, Synthesis, characterisation and photocatalytic activity of different metal-doped titania systems, *Appl. Catal. A.*, 2006, **306**, 120–127.

60 L. Lhomme, S. Brosillon, D. Wolbert, J. Photochem. Photocatalytic degradation of a triazole pesticide, cyproconazole, in water, *Photobiol.*, 2007, **188**, 34–42.

61 Y. Zhou, W. Chen, D. Wang, Mononuclear, dinuclear, hexanuclear, and one-dimensional polymeric silver complexes having ligand-supported and unsupported argentophilic interactions stabilised by pincer-like 2,6-bis(5-pyrazolyl)pyridine ligands, *Dalton Trans.*, 2008, **11**, 1444–1453.

62. M. Fukui, H. Kouda, A. Tanaka, K. Hashimoto, H. Kominami, Heterogeneous meerwein-ponndorf-verley–type reduction of aromatic aldehydes having other reducible functional groups over a TiO_2 photo-catalyst, *ChemistrySelect*, 2017, **2**, 2293-2299.

Supplementary material to:

V. Moodley, S. Maddila, S.B. Jonnalagadda and W.E. van Zyl

Degradation of *o*-chloranil using nanocrystalline-cellulose/TiO_2 composites *via* a solar photocatalytic route

S. Afr. J. Chem., 2021, **75**, 91–97

SUPPLEMENTARY MATERIAL

Degradation of *o*-chloranil using nanocrystalline-cellulose/TiO_2 composites *via* a Solar Photocatalytic Route

Vashen Moodley, Suresh Maddila, Sreekantha B. Jonnalagadda and Werner E. Van Zyl*

School of Chemistry and Physics, University of KwaZulu-Natal, Westville campus, Chiltern Hills, Durban, 4000, South Africa.

Contents **Page number**

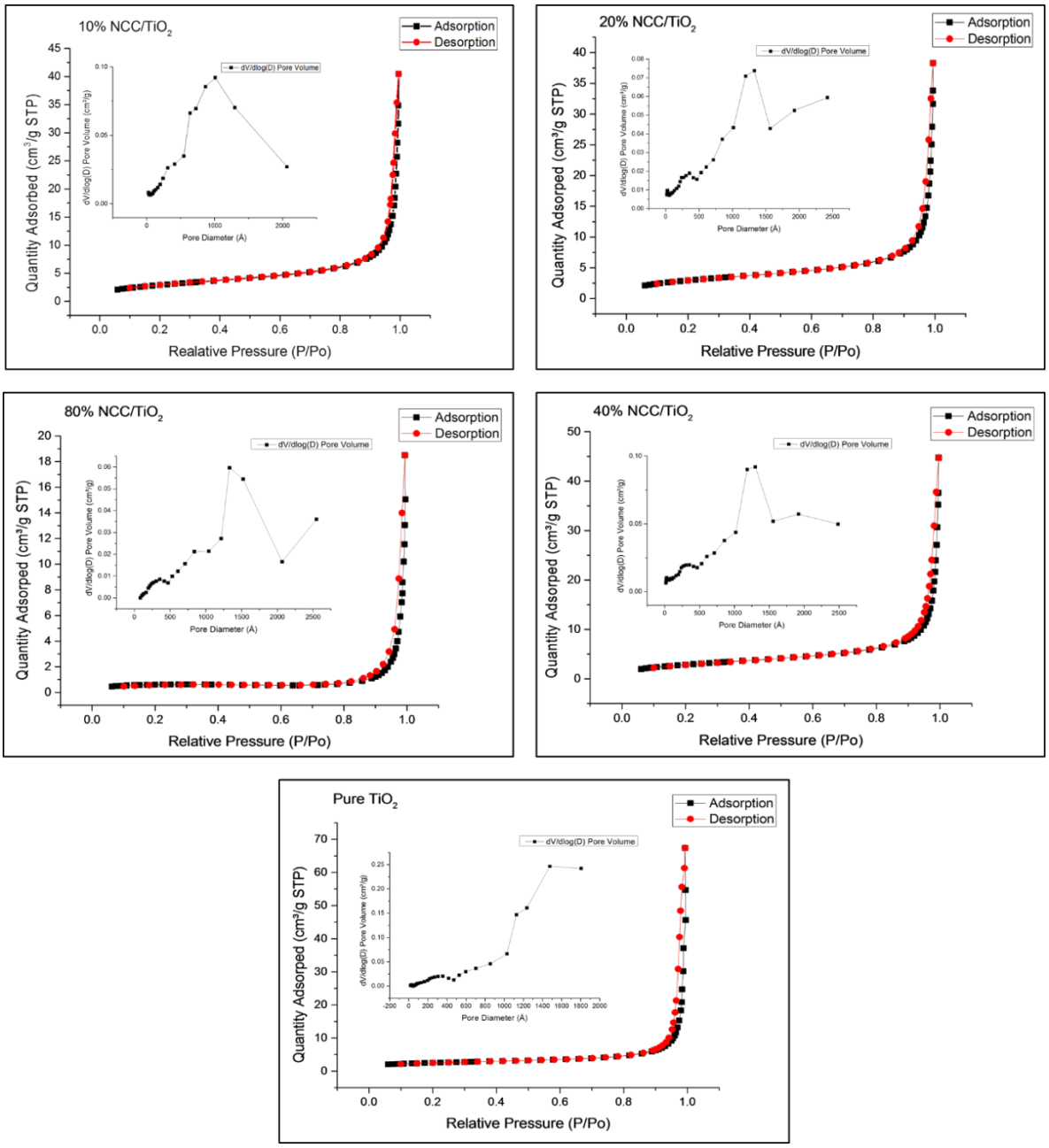

Figure S1. N_2 adsorption-desorption isotherm plots of synthesized catalysts with pore volume density (insets).

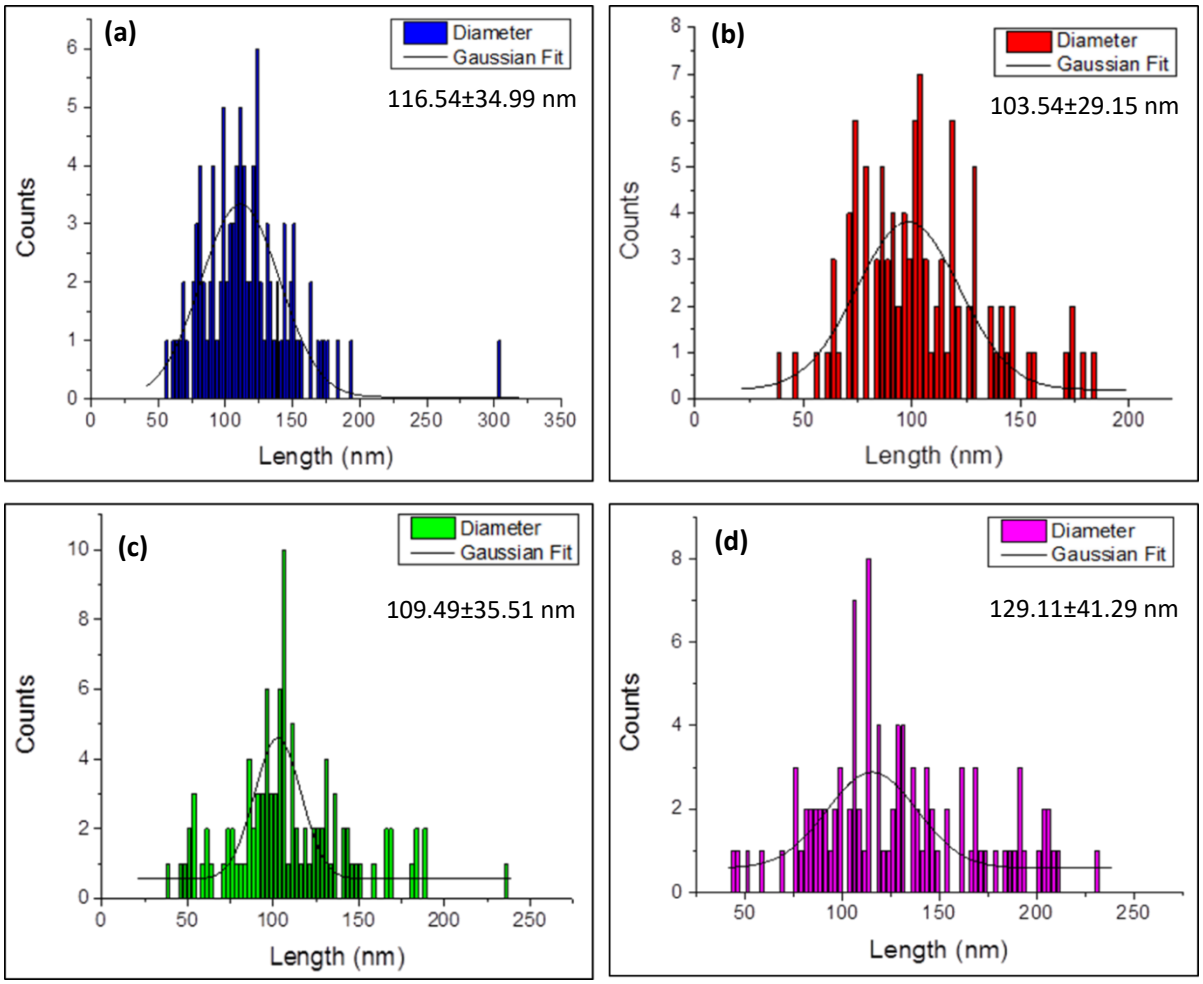

Figure S2. Particle size distribution graphs of 10% (a), 20% (b), 40% (c) and 80% (d) NCC/TiO_2 catalysts

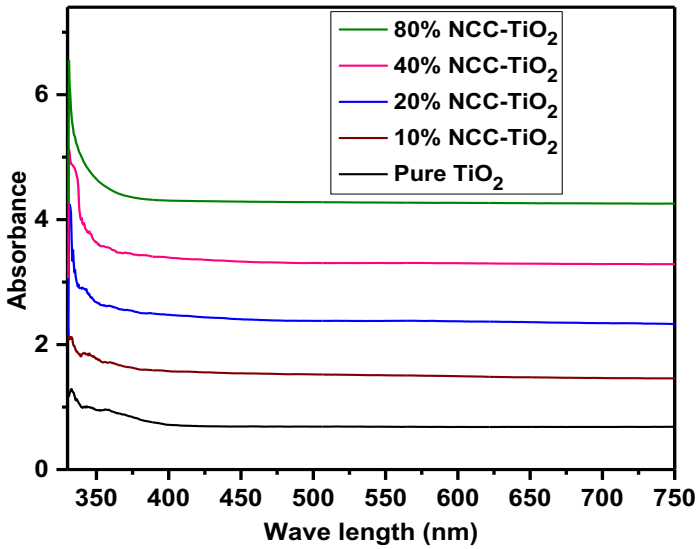

Figure S3. UV-DRS of bare TiO_2 and synthesized (% w/w) NCC doped TiO_2 catalysts.

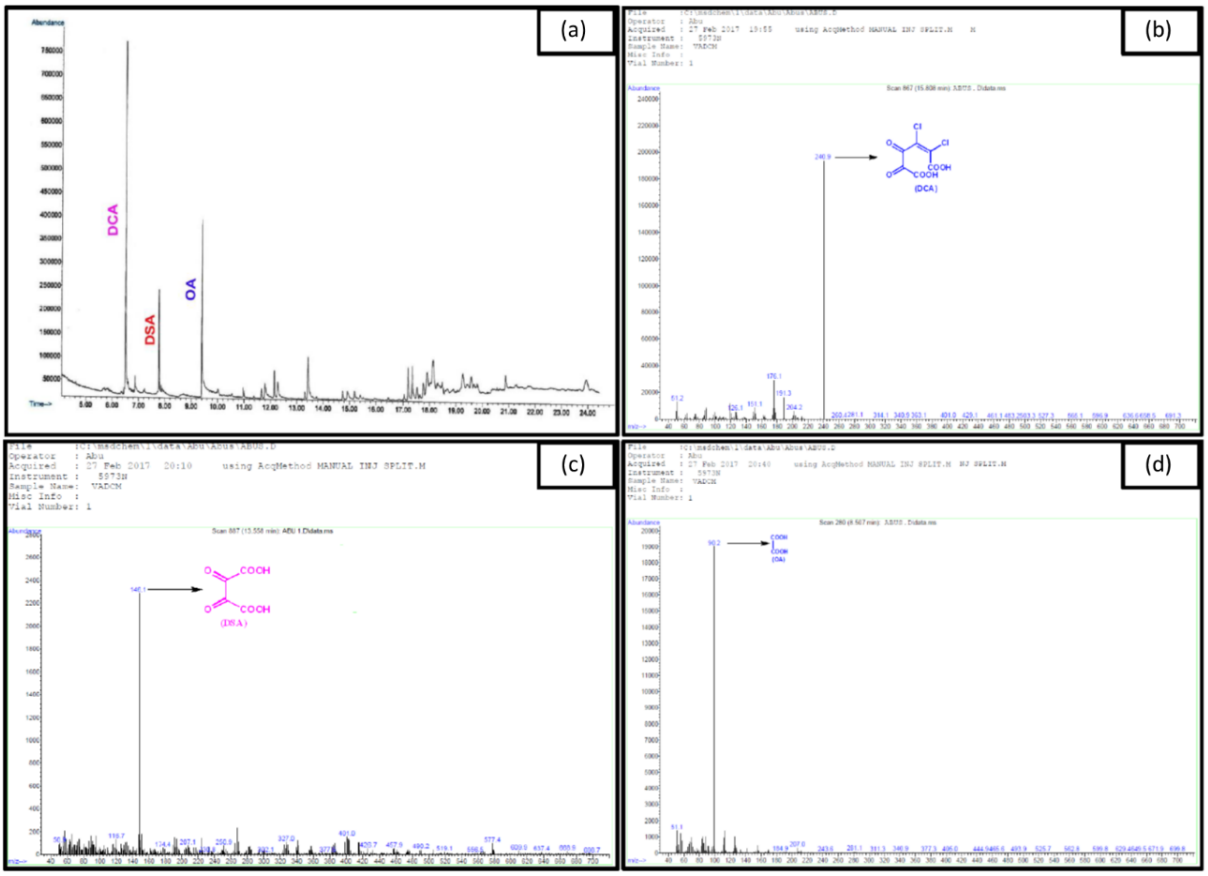

Figure S4. Degradation products confirmed by Gas Chromatography (S4a) and LC mass spectra of degradation products (S4b, S4c and S4d).